Available online at www.sciencedirect.com
ScienceDirect
Journal of Molecular Catalysis A: Chemical 267 (2007) 79–85
JOURNAL OF MOLECULAR CATALYSIS A: CHEMICAL
www.elsevier.com/locate/molcata

Preparation and characterization of a titanium-substituted hydroxyapatite photocatalyst

Hu Anmin *, Li Ming, Chang Chengkang, Mao Dali

The State Key Laboratory of the Metal Matrix Composites, School of Materials Science and Engineering, Shanghai Jiaotong University, Shanghai 20030, China

Received 26 December 2005; received in revised form 15 November 2006; accepted 21 November 2006
Available online 26 November 2006

Abstract

Nanocrystals of titanium-substituted hydroxyapatite (CTHAp) were prepared with Ti^{4+} concentrations of $x = 0$, 0.1, 0.2 and 0.5 [$x = Ti/(Ca + Ti)$] at hydrothermal temperatures of 100, 150, 190 and 230 °C. The effects of reaction temperature and titanium concentration on the crystal were investigated by using TEM, XRD, FTIR, ICP and XPS. The obtained CTHAp crystallites were rod like pure hydroxyapatite phase (about 70 nm in length and 10 nm in diameter), the crystallinity and grain sizes decreased with the increase of XTi, and increased with hydrothermal temperature from 100 to 230 °C. The concentration of Ti^{4+} near the surface is larger than in the bulk. The photocatalytic activity of CTHAp was examined by using decomposition of methylene blue (MB) and found that CTHAp had good photocatalytic activity under visible light and UV irradiation.

Keywords: Hydrothermal synthesis; Hydroxyapatite; Titanium; Photocatalyst

1. Introduction

One of the most important challenges for science is to develop efficient methods to control environmental pollution. The TiO_2 catalyst exhibits good activity for photo-oxidation of organic compounds when either oxygen or liquid oxidants are used [1,2]. It is also chemically stable, commercially available, and inexpensive. For practical applications, however, there are some difficulties such as either filtration of fine TiO_2 or fixation of catalyst particles and effective utilization of UV rays. Several attempts have been made to increase its photoefficiency either by noble metal deposition [3] or by ion doping [4,5], other way to increase the photocatalytic efficiency of titania consists of adding a coadsorbent such as silica, alumina, zeolites, activated carbon or clays [6–9]. But, there were need important improvement of photoefficiency under UV irradiation and especially under visible light irradiation.

Hydroxyapatite (HAp) is known as not only a primary constituent of the biological hard tissues but also adsorbents and catalysts [10–12]. The surface-OH groups adsorb CO_2, NOx, H_2O, organic compounds and excellent affinity to biomaterials such as proteins. It was found that the oxidative decomposition of odor compounds such as methyl mercaptane (MM) and dimethyl sulfide (DMS) occurred effectively on HAp under UV (254 nm) irradiation [13–16]. It was also found that HAp treated with Ag^+ had the structure of $(Ag,Ca)_{10}(PO_4)_6(OH)_2$ which exhibited good antimicrobial effects[17]. Wakamura. M. and Komazaki, Y. found when the HAp particles penetrated by Ti^{4+} into the crystals by coprecipitation methods, the Ti(IV)-modified HAp [$(Ti,Ca)_{10}(PO_4)_6(OH)_2$, CTHAp] can absorb UV beam at a wavelength less than 380 nm and exhibits a higher bactericidal effect and decomposition of acetaldehyde than TiO_2 both in the dark and under UV irradiation. But with more Ti(IV) modified ($Ti/(Ca + Ti) > 0.1$), the product CTHAp is poorly crystallized and the efficient of photocatalysis is poor also [18,19].

In the present paper, we propose a low-temperature hydrothermal method through which CTHAp crystals were highly crystallized, and the compositional, structural, morphological analyses and photocatalytic properties were studied.

2. Experimental methods

2.1. Materials

The starting materials were analytical grade: $Ca(NO_3)_2$, $NH_4H_2PO_4$, NH_4OH, and $TiCl_4$. $TiCl_4$ was added to the

* Corresponding author.
E-mail address: huanmin@tsinghua.org.cn (A. Hu).

1381-1169/$ – see front matter © 2006 Elsevier B.V. All rights reserved.
doi:10.1016/j.molcata.2006.11.038

$Ca(NO_3)_2$ solution to produce (Ca + Ti) solution, using Ti^{4+} concentrations of $x = 0$, 0.1, 0.2 and 0.5 with respect to the total metal ion concentration [x = Ti/(Ca + Ti)], noted as CTHAp-0, CTHAp-1, CTHAp-2 and CTHAp-5. Colloidal CTHAp powders were produced by dropped $NH_4H_2PO_4$ solution into (Ca + Ti) solution at pH adjusted to 9.1 with ammonium hydroxide. The precipitate formed during the reaction was filtered and washed with distilled water. CTHAp crystal was synthesized by adding 2.0 g colloidal CTHAp powder with distilled water into 200 ml teflon container at pH adjusted to 9. After the mixture was stirred well, the container was tightly sealed in a stainless steel autoclave and put in an oven at 100, 150, 190 and 230 °C for 8 h. The autoclave was cooled down to a room temperature, then, the products were filtered and washed with distilled water. The products were filtered and washed with distilled water, finally dried in an air oven at 80 °C for 24 h.

2.2. Characterization of catalyst

The crystalline phases of the reaction products were identified by powder X-ray diffraction (XRD) analyses using a Rigaku D/MAX-IIIA diffractometer with Cu Ka radiation ($\lambda = 0.15418$ nm). The accelerating voltage of 35 kV and emission current of 30 mA were applied. The specific surface areas were measured by the Brunauer–Emmett–Teller (BET) method, in which the N_2 adsorption at 77 K using an ASAP 2010M + C Sorptometer. The morphology, particle size and size distribution of particles was investigated by a Jeol 100CXII transmission electron microscopy (TEM). Fourier transform infrared spectra of the samples were recorded with a FTIR spectrometer (EQUINOX55) at room temperature. The element analysis was carried out by inductively coupled plasma atomic emission spectrometry ICP (IRIS ADVANTAGE/1000) and EDS (JEM2100F, 20 kV). The element concentrations in the depth direction were measured by AES (PHI550ESCA/SAM, 1.5 KeV).

2.3. Characterization of photocatalytic activity

The diffuse reflectance UV–vis spectra of the solid powder materials were measured on a UV–vis spectrophotometer (HITACHI, U-3010). Photocatalytic activity was evaluated from the decomposition of methylene blue (guaranteed reagent grade, $C16H18N3S$, MB) in its aqueous solution with 1.0×10^{-5} mol/l concentration at room temperature (20 °C), 200 mg CTHAp were added under stirring in 40 ml MB solution in 50 ml beaker and maintained in the dark during 1 h to reach a complete adsorption at equilibrium, and then irradiated by ultraviolet rays (UV) and visible light (vis). A 300 W Xe arc lamp (Philips) with a cutoff filter ($\lambda > 400$ nm) used as a visible light source and a 300 W high pressure Hg lamp (Philips) used as a UV light source ($\lambda_{max} = 365$ nm) were positioned up the beaker with distance of 40 cm with water cooling system to prevent the thermal catalytic effect. During adsorptivity and photoactivity measurements, MB solution was stirred by using a magnet at the bottom of the beaker. Change in concentration of MB in solution either due to adsorption and decomposition was determined from the relative absorbance at a wavelength of 662 nm in UV–vis spectrum by using the Equation $x = C/C_0 = A/A_0$ [20–22].

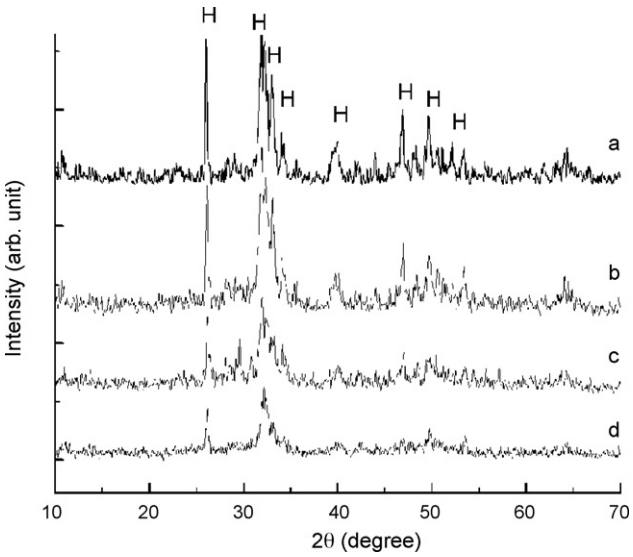

Fig. 1. XRD patterns of the samples (a) CTHAp-0, (b) CTHAp-1, (c) CTHAp-2, (d) CTHAp-5 hydrothermal synthesized at 190 °C for 8 h.

3. Results and discussion

Fig. 1 reports the powder XRD patterns of the products in the presence of different amounts of Ti^{4+} ions in solution hydrothermal synthesized at 190 °C for 8 h. Pure hydroxyapatite phase were obtained in all samples. As the amount of Ti^{4+} increased, the intensity of diffraction peaks is weakened and half height width (HHW) of major diffraction peaks is widened upon increasing XTi, this indicated a low crystallinity of the CTHAp powders compared to the pure HAp [23-26].

Fig. 2 shows that the (0 0 2) reflections of powders containing Ti^{4+} shifted to higher angles by increasing the Ti content, this

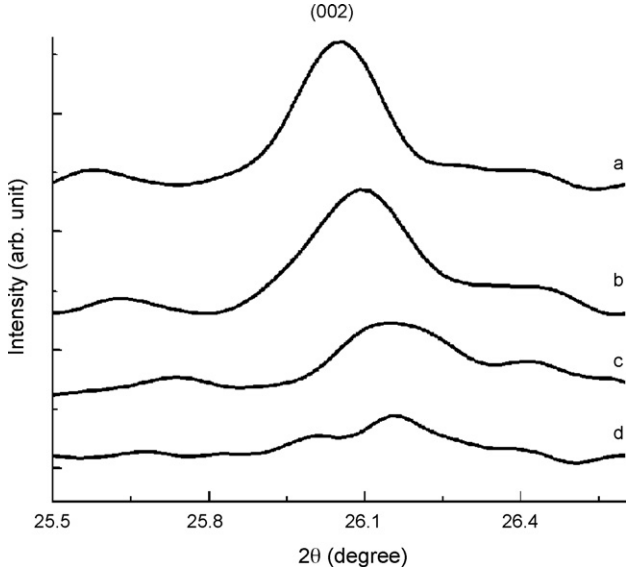

Fig. 2. (0 0 2) peak reflections of the samples (a) CTHAp-0, (b) CTHAp-1, (c) CTHAp-2, (d) CTHAp-5 hydrothermal synthesized at 190 °C for 8 h.

Table 1
Unit cell parameters of the CTHAp samples

Sample	a, b (nm)	c (nm)	V (nm^3)
CTHAp-0	0.9441	0.6881	0.5311
CTHAp-1	0.943	0.6873	0.5292
CTHAp-2	0.9422	0.6865	0.5277
CTHAp-5	0.9413	0.6857	0.5261

Notes: a, b, c are lattice parameters; V is primitive cell volume.

indicates that the Ca^{2+} cations were substituted by Ti^{4+} in the CTHAp structure. Table 1 shows that the lattice parameters a, b and c and cell volume decreased with the increasing of Ti content. This confirmed that with Ti^{4+} substitution increase, lattice disorder associated in the HAp lattice increase too. It is well known divalent ions smaller than Ca^{2+}, such as Mg^{2+}, Zn^{2+} and Mn^{2+} have a similar inhibitory effect, and this substitution of the smaller sized ion gives rise to lattice strain [23,24]. On the contrary, divalent ions larger than Ca^{2+}, such as Sr^{2+} and Ba^{2+}, are known to easily substitute for Ca^{2+} in HAp [23–28]. While, Wakamura found in the HAp substituted with trivalent ions, such as Al(III), La(III) and Fe(III), which smaller than Ca^{2+}, did not according to this rule, these trivalent ions accelerated the growth of HAp particles, markedly for Fe(III) [26]. Quadrivalent ions Ti^{4+} have smaller radii (0.075 nm) than 0.099 nm of Ca^{2+}, although the charge of Ti^{4+} ions is different from divalent ions, calcium hydroxyapatite modified with Ti^{4+} was also difficult to obtain high crystallinity, and greatly inhibit hydroxyapatite crystallization, the same as the divalent ions.

Fig. 3 compares XRD patterns of the CTHAp-2 powder obtained at 100, 150, 190 and 230 °C hydrothermal temperatures. As the hydrothermal temperatures increased, the

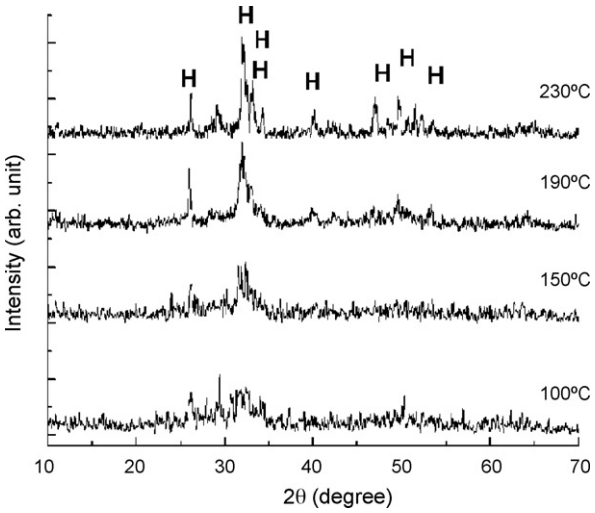

Fig. 3. XRD patterns of CTHAp-2 powders hydrothermal synthesized at 100, 150, 190 and 230 °C for 8 h.

grain sizes and the crystallinity of the apatite phase increased [23–26].

Fig. 4 shows the TEM pictures of the particles formed with different titanium concentrations at hydrothermal temperatures of 190 °C for 8 h. As seen in Fig. 4, all samples have the rod-shaped appearances. Fig. 4(a) micrographs indicate that rod-like CTHAp-0 crystals are approximately 70 nm in length and 10 nm in diameter. As Ti^{4+} content increased, the particles of CTHAp-1 and CTHAp-2 become smaller, with approximately 50–70 nm in length and 6–9 nm in diameter. The sample CTHAp-5 has the smallest crystals, but the crystallinity of the samples decreased greatly. To obtain high crystallinity CTHAp-5, we increased

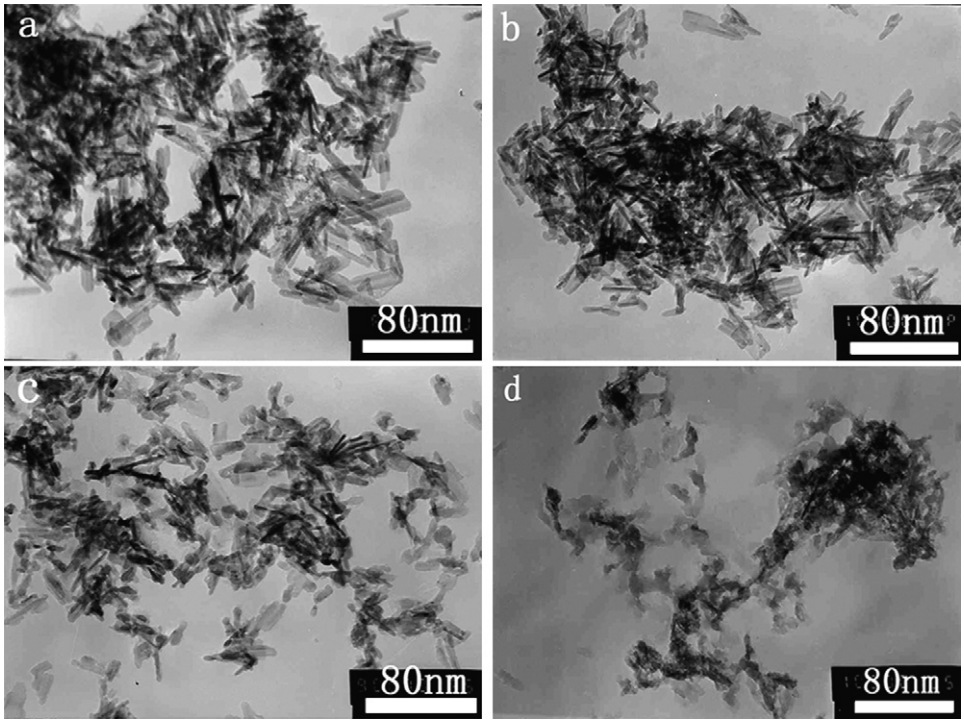

Fig. 4. TEM images of samples (a) CTHAp-0, (b) CTHAp-1, (c) CTHAp-2, (d) CTHAp-5 hydrothermal synthesized at 190 °C for 8 h.

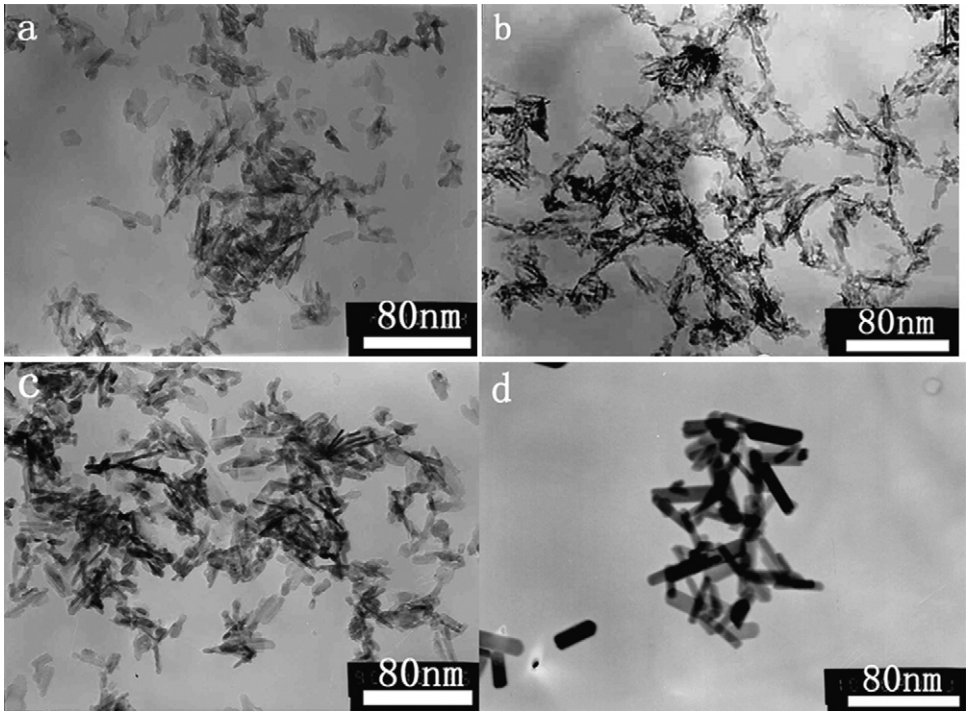

Fig. 5. TEM images of CTHAp-2 powders synthesized at (a) 100, (b) 150 °C, (c) 190 and (d) 230 °C for 8 h.

hydrothermal temperature to 230 °C, but the results are almost the same. This means that it is difficult to obtain high crystallinity CTHAp-5 at 190 and 230 °C for 8 h. This may be the lattice disorder associated with increasing Ti^{4+} substitution in the HAp lattice.

Fig. 5 shows the TEM pictures of the sample CTHAp-2 hydrothermal at different temperatures for 8 h. As seen in Fig. 5, as hydrothermal temperatures increased from 100 to 230 °C, the grain size and the crystallinity of the rod-shaped particles increased. Some authors also found that hydrothermal temperatures have a great influence on the grain sizes and the crystallinity of the apatitic phase. The higher temperatures the larger grain sizes and higher crystallinity are obtained [17–19].

FTIR spectra of the CTHAp powders with different amounts of Ti^{4+} ions content are shown in Fig. 6. These are typical spectra of HAp showing PO_4^{3-} derived bands at 478, 566, 605, 963, and 1030–1090 cm^{-1} and adsorbed water bands at 1630 and 3000–3700 cm^{-1} [23–26]. Low intensity of both OH-derived bands at 630 and 3570 cm^{-1} are only clearly visible in the nominally stoichiometric HAp powder. With increasing the Ti^{4+} concentration, it can be observed that the intensity of the peaks associated with phosphate bands was reduced. These effects can be explained by decrease of crystallinity due to increased Ti substitution in the HAp lattice.

To determine the composition of the products by the hydrothermal synthesis, CTHAp compound (hydrothermal synthesized at 190 °C for 8 h) were analyzed by ICP and EDS, the results are shown in Table 2 and Fig. 7. Taking account of the charge balance of CTHAp crystal, the substitution ratio for the exchange of Ca^{2+} with Ti^{4+} ions should be 4:2 = 2. Calculated by (Ca + 2Ti)/P, The ratio after Ti^{4+} substitution is 1.79–2.27 which is larger than the theoretical ratio (1.67), and the departure ratio increase with the increase of XTi. This mean that the charge is not balanced in the substitution by Ti^{4+}. Thus, to keep the charge balance, Ti^{4+} ions would be incorporated into the particles as lower valence ions or as hydroxo ions: $Ti(OH)_3^+$ or $Ti(OH)_2^{2+}$. The existence of these hydroxo ions in the powers and more in the surface layer would reduce the intensity of the peaks associated with phosphate bands [18,19].

The surface structure and properties CTHAp are fundamentally important in catalysts fields and the usage of this material.

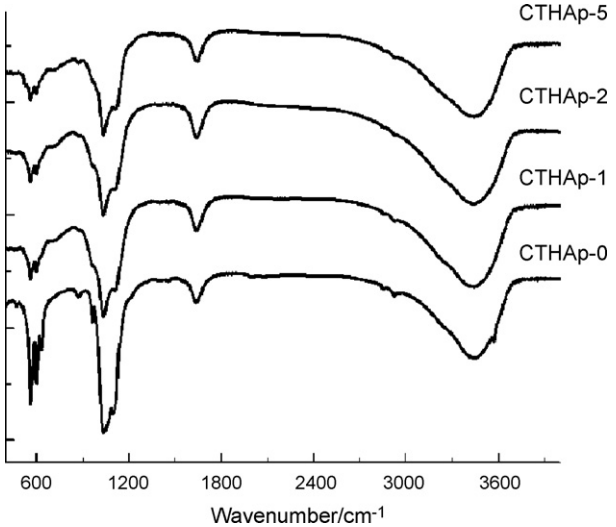

Fig. 6. FT-IR spectra of CTHAp powders hydrothermal synthesized at 190 °C for 8 h.

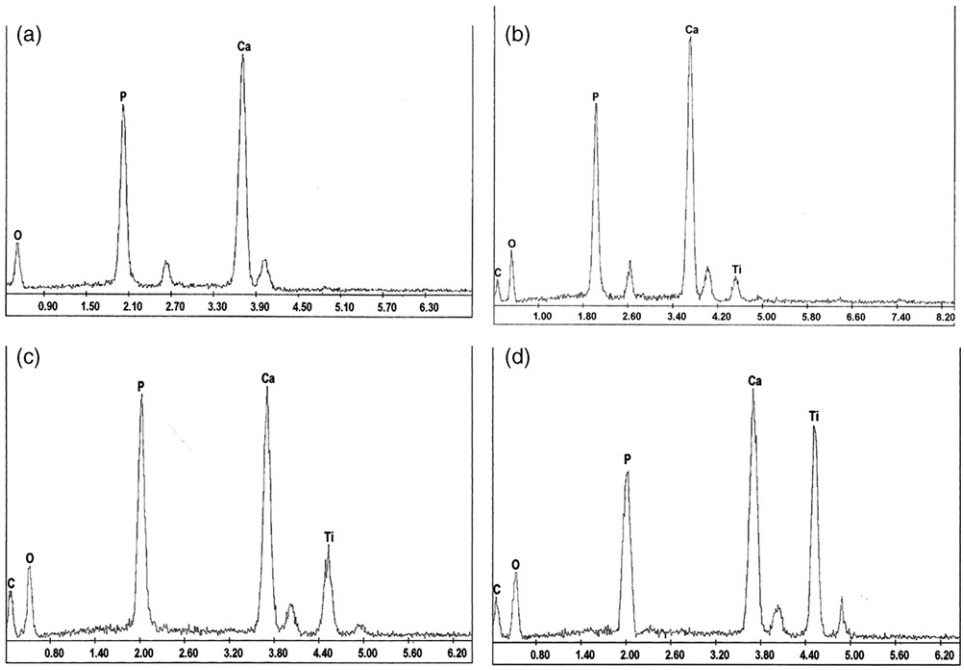

Fig. 7. EDS results of samples (a) CTHAp-0, (b) CTHAp-1, (c) CTHAp-2 and (d) CTHAp-5 hydrothermal synthesized at 190 °C for 8 h.

Table 2
Composition of CTHAp powders analyzed by ICP

Sample	Ca (wt.%)	P (wt.%)	Ti (wt.%)	Ti/(Ca + Ti)	(Ca + 2Ti)/P
CTHAp-0	35.67	16.54	–	–	1.67
CTHAp-1	31.62	16.17	3.42	0.08	1.79
CTHAp-2	27.63	16.05	7.92	0.19	1.98
CTHAp-5	15.84	15.17	17.13	0.47	2.27

In this study, AES measurements were performed in an attempt to elucidate any Ti enrichment near the surface of CTHAp-2 powder (hydrothermal synthesized at 190 °C/8 h). The results (Fig. 8) indicate that the distribution of Ti^{4+} ion. Close to the surface of the crystals (3–10 nm depth) was about 6 at.%, which is larger than 4.5 at.% inside the crystals (20–30 nm depth). This

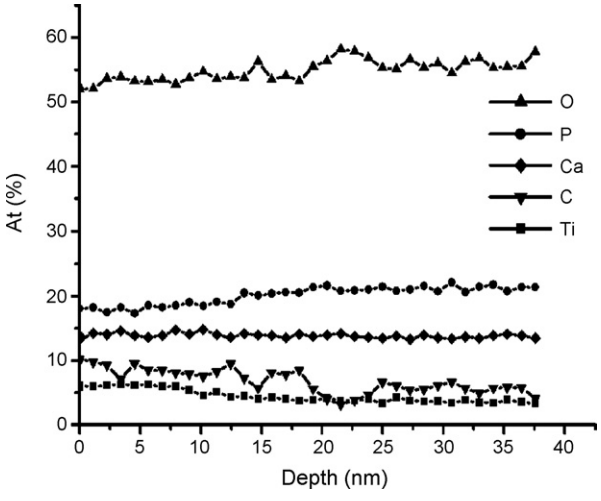

Fig. 8. AES results of CTHAp-2 powders.

indicates that the Ti ion probably just a part of Ti^{4+} ions is substituted for calcium, the remainder being adsorbed on the crystal surface, this result is conformed with FT-IR spectra analysis.

Position of the metal ion in HAp is a subject of much controversy. There are several works, which reported presence of Mg^{2+} on the surface of HAp crystals [24]. Conversely, W L. Suchanek found the concentration of Mg was slightly lower near the surface than in the bulk of the HAp crystals. They thought that some of the Mg ions in the near-surface positions could have been leached out during the purification process, resulting in lower Mg concentration near the surface than in the bulk [24]. Wakamura found the particles modified with Ni^{2+} and Cu^{2+} was much less than the atomic ratio of the whole particle, while the concentration of Cr^{3+} near the surface modified with Cr^{3+} approximated to the bulk [26].

BET surface areas of CTHAp-2 (hydrothermal synthesized at 190 °C/8 h) are presented in Table 2. The BET surface areas of the CTHAp compound decrease from 127.2 to 217.3 m^2/g as the Ti^{4+} content was increased from $x = 0$ to 0.5.

The diffuse reflectance UV–vis spectra of the CTHAp photocatalysts are shown in Fig. 9. As expected, nano-TiO_2 (SBET = 152.8 m^2/g) has no absorption above its fundamental absorption sharp edge rising at about 370–380 nm [1,2], while pure hydroxyapatite (CTHAp-0) has no absorption above 250 nm. Rulis et al. [29] found that the calcium apatites [$Ca_{10}(PO)_4X_2$] with X = (OH^-, F^-, Cl^-, or Br^-) are all band-gap insulators and the band gaps are about 5.3 eV. This means that absorption edge of HAp may appear at 230 nm. On the other hand, HAp with Ti^{4+} substituted, the CTHAp catalysts can absorb at higher wavelengths than that of HAp and TiO_2. An apparent enhancement of absorption is observed for the CTHAp-1 catalyst, and the absorption is totally over the whole range of the UV–vis spectrum for CTHAp-2 and CTHAp-5.

Table 3
BET surface area and photocatalytic properties of CTHAp powders

Sample	CTHAp-0	CTHAp-1	CTHAp-2	CTHAp-5	TiO_2
SBET (m^2/g)	142.7	150.4	161.6	177.3	152.8
After 1 h in dark (C/C_0)	0.86	0.85	0.83	0.83	0.94
After 2 h in dark (C/C_0)	0.86	0.83	0.82	0.81	0.93
After 1 h under vis (C/C_0)	0.84	0.66	0.45	0.51	0.90
After 1 h under UV (C/C_0)	0.76	0.44	0.32	0.39	0.31

It is noticeable that the enhancements of absorption increase with the increase Ti^{4+} content in the CTHAp. According to the composition analyzed, there are excess Ti^{4+} ions in the CTHAp which may indicate an increment of surface electric charge of the CTHAp [30], and enhance the absorption.

The photocatalytic activity of CTHAp powders hydrothermal synthesized at 190 °C for 8 h were assessed by the degradation experiment of MB aqueous solution in dark, under visible light and UV irradiation, the results are shown in Table 3. After 1 h in the dark, about 15–17% MB were absorbed by CTHAp and only 7% were absorbed by TiO_2, another 1 h in the dark, the concentration of MB change little. This means that CTHAp or TiO_2 has little photocatalytic activity in the dark and can reach complete adsorption equilibrium after 1 h in the dark.

After 1 h photodegradation reaction excitated by visible light and UV irradiation, CTHAp-0 (pure HAp) nanocrystallines have slight photocatalytic activity under UV irradiation [14,29]. While 17–37% and 39–50% MB were destroyed by CTHAp-1, CTHAp-2 and CTHAp-5 under 1 h visible light and UV irradiation. These results show that all nanocrystallines CTHAp have the photocatalytic activity both under visible light and UV irradiation, the photocatalytic activity of HAp was excitated by titanium substituted (CTHAp). Correspondingly, nano-TiO_2 have hardly any photocatalytic activity (0–3%) under visible light irradiation, but they have higher photocatalytic activity (∼60%) under UV [1,2]. It can see that among all CTHAp samples, CTHAp-2 has the best photocatalytic activity, this mean the photocatalytic activity may be related not only with XTi, but also with the particle size, crystalline quality, morphology, specific surface area, surface state, etc.

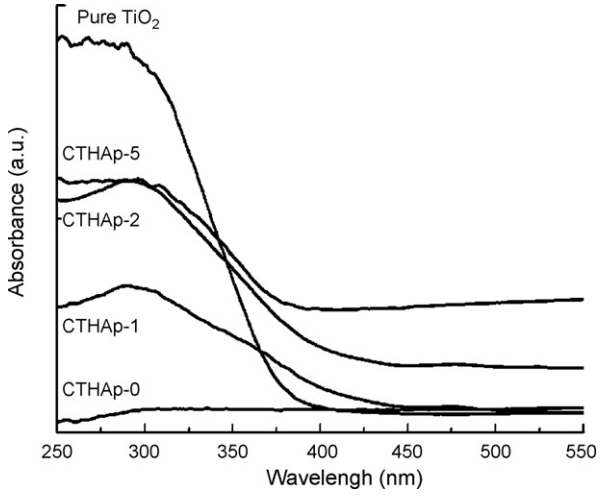

Fig. 9. Diffuse reflectance UV–vis spectra of the CTHAp photocatalysts.

4. Conclusion

Rod-like CTHAp Nanocrystals were prepared with different titanium concentrations at different hydrothermal temperatures. All the materials were pure hydroxyapatite phase. At higher hydrothermal temperatures and with increasing titanium substitution, the crystallinity of CTHAp was higher. UV–vis spectra of the solids indicate that the enhancements of absorption increase with the increase Ti^{4+} substitution from 0.1 to 0.5 of the CTHAp catalyst. The photocatalytic properties of CTHAp have been observed by on the photocatalytic degradation of MB. Although the CTHAp catalysts with different XTi show comparable adsorption capacities in the range of UV–vis spectra, the higher photocatalytic activity is observed when XTi increase from 0 to 0.2 which favors the MB disappearance. These means that the photocatalytic properties of CTHAp may be related with the particle size, crystalline quality, morphology, specific surface area and surface state.

Acknowledgements

This work was financially supported by Shanghai Nanotechnology Promotion Center (Contract no. 0352nm062) and China Postdoctoral Science Foundation (Contract no. 37).

References

[1] H. Nishikawa, S. Kato, T. Ando, J. Mol. Catal. A Chem. 236 (2005) 145.
[2] M.S. Lee, S.S. Hong, M. Mohseni, J. Mol. Catal. A Chem. 242 (2005) 135.
[3] X.F. You, F. Chen, J.L. Zhang, M. Anpo, Catal. Lett. 102 (2005) 247.
[4] B. Zielinska, A.W. Morawski, Appl. Catal. B Environ. 55 (2005) 221.
[5] M. Mrowetz, W. Balcerski, A.J. Colussi, J. Phys. Chem. B 108 (2004) 17269.
[6] J. Matos, J. Laine, J.M. Herrmann, J. Catal. 200 (2001) 10.
[7] T. Nakajima, Y.H. Xu, Y. Mori, M. Kishita, H. Takanashi, S. Maeda, A. Ohki, J. Hazard. Mater B120 (2005) 75.
[8] E.P. Reddy, L. Davydov, P. Smirniotis, Appl. Catal. B Environ. 42 (2003) 1–11.
[9] M. Mohseni, Chemosphere 59 (2005) 335.
[10] R. Kumar, K.H. Prakash, P. Cheang, K.A. Khor, Acta Mater. 53 (2005) 2327.
[11] F. Herve, F. Fouache, C. Marche, J.P. Tillement, J. Chromatogr. B 688 (1997) 35.
[12] S. Bailliez, A. Nzihou, J. Chem. Eng. 98 (2004) 141.
[13] N. Harumitsu, K. Shinji, A. Takahiro, J. Mol. Catal. A Chem. 236 (2005) 145.
[14] H. Nishikawa, K. Omamiuda, J. Mol. Catal. A Chem. 179 (2002) 193.
[15] H. Nishikawa, J. Mol. Catal. A Chem. 206 (2003) 331.

[16] H. Nishikawa, J. Mol. Catal. A Chem. 207 (2004) 149.
[17] Q.L. Feng, F.Z. Cui, T.N. Kim, J.W. Kim, J. Mater. Sci. Lett. 18 (1999) 559.
[18] M. Wakamura, K. Hashimoto, T. Watanabe, Langmuir 19 (2003) 3428.
[19] Y. Komazaki, H. Shimizu, S. Tanaka, Atmos. Environ. 33 (1999) 4363.
[20] X.Y. Chuan, M. Hirano, M. Inagaki, Appl. Catal. B Environ. 51 (2004) 255.
[21] S. Kaneco, M.A. Rahman, T. Suzuki, H. Katsumata, K. Ohta, J. Photochem. Photobiol. A 163 (2004) 419.
[22] J. Matos, J. Laine, J.M. Herrmann, Appl. Catal. B Environ. 18 (1998) 281.
[23] H.G. McCann, J Biol. Chem. 201 (1953) 247.
[24] W.L. Suchanek, K. Byrappa, P. Shuk, R.E. Riman, V.F. Janas, K.S. Ten-Huisen, Biomaterials 25 (2004) 4647.
[25] Z.D. Feng, Y.M. Liao, M. Ye, J. Mater. Sci. Mater. Med. 16 (2005) 417.
[26] M. Wakamura, K. Kandori, T. Ishikawa, Colloid. Surf. A 164 (2000) 297.
[27] E. Bertoni, A. Bigi, G. Cojazzi, M. Gandolfi, S. Panzavolta, N. Roveri, J. Inorg. Biochem. 72 (1998) 29.
[28] M. Hidouri, K. Bouzouita, F. Kooli, I. Khattech, Mater. Chem. Phys. 80 (2003) 496.
[29] P. Rulis, L.Z. Ouyang, W.Y. Ching, Phys. Rev. B 70 (2004) 155104.
[30] W.D. Wang, P. Serp, P. Kalck, J.L. Fari, Appl. Catal. B Environ. 56 (2005) 305.